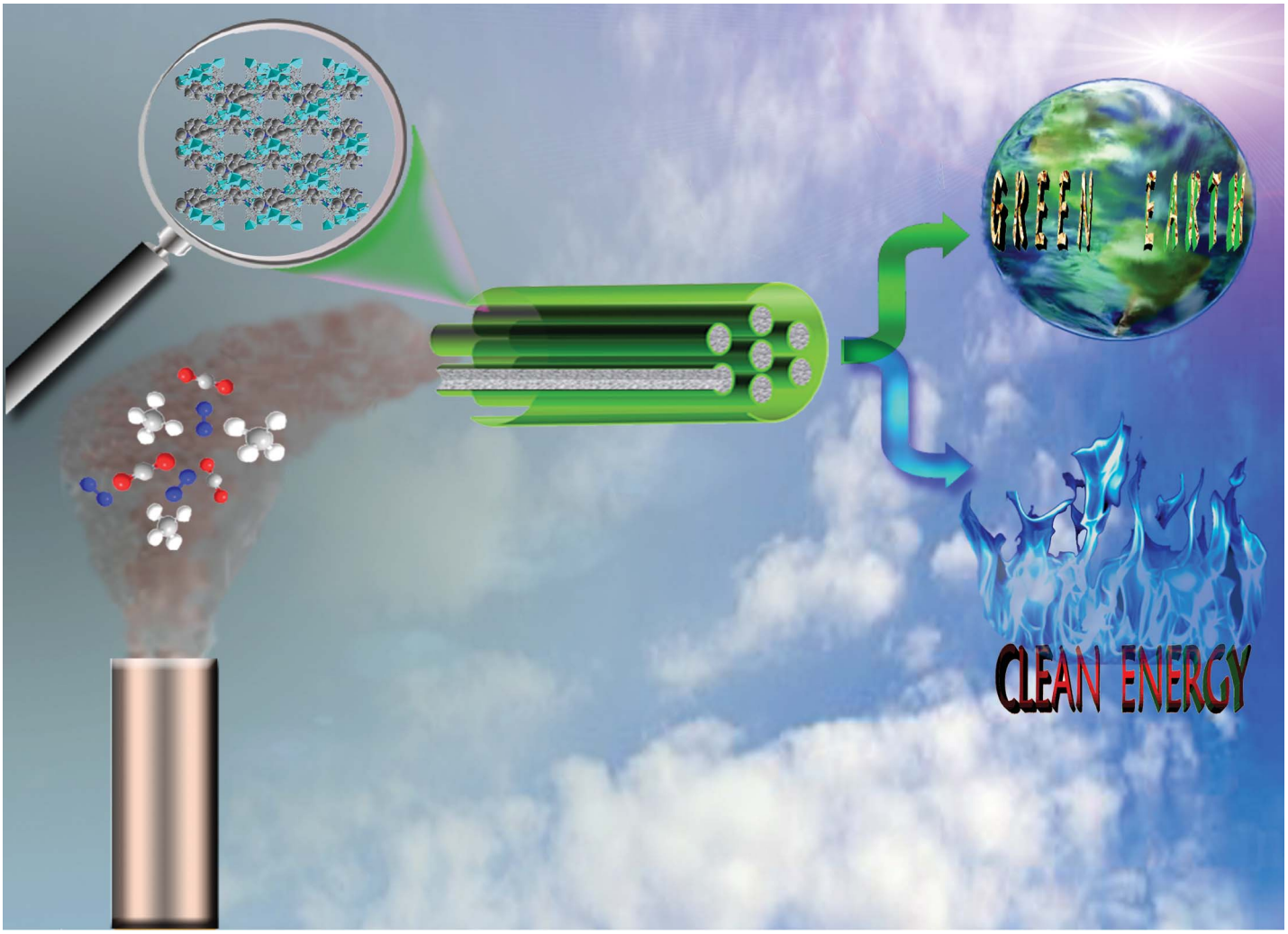

Showcasing research from College of Engineering, Peking University.

Title: Selective adsorption of CO_2/CH_4 and CO_2/N_2 within a charged metal–organic framework

A novel charged metal–organic framework material is obtained with ultramicroporous structures and appropriate pore chemical environments tailored for CO_2 capture and separation.

As featured in:

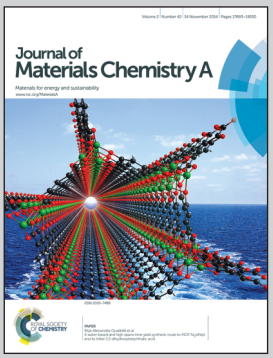

See Ruqiang Zou *et al.*, *J. Mater. Chem. A*, 2014, **2**, 17771.

ROYAL SOCIETY OF CHEMISTRY

www.rsc.org/MaterialsA

Registered charity number: 207890

Journal of Materials Chemistry A

PAPER

View Article Online
View Journal | View Issue

Cite this: J. Mater. Chem. A, 2014, 2, 17771

Selective adsorption of CO_2/CH_4 and CO_2/N_2 within a charged metal–organic framework†

Lidan Kong,[a] Ruyi Zou,[c] Wenzhu Bi,[c] Ruiqin Zhong,[b] Weijun Mu,[a] Jia Liu,[a] Ray P. S. Han[a] and Ruqiang Zou*[a]

Received 22nd April 2014
Accepted 1st August 2014

DOI: 10.1039/c4ta01993h

www.rsc.org/MaterialsA

Presented here is a new ultramicroporous metal–organic framework (MOF) formulated as $[Zn_3L_2(HCOO)_{1.5}][(CH_3)_2NH_2]_{1.5}\cdot x$DMF, **1** ($H_3L$ = 9-(4-carboxy-phenyl)-9*H*-carbazole-3,6-dicarboxylic acid), DMF = *N*,*N*-dimethylformamide, consisting of an anionic framework and two types of interlaced one-dimensional channels with 0.42 and 0.79 nm diameters respectively, in which the larger channels accommodate protonated dimethylamine as the counter cations. Gas sorption analysis of N_2, CO_2 and CH_4 was investigated and the isotherms exhibit reversible thermodynamic behaviours without hysteresis desorption, evidencing framework rigidity and permanent porosity of solvent-free **1**. The synergistic effect of the open ultramicropores and dimethylamine cations may lead to high efficiency separation of CO_2 from CH_4 and N_2. According to the Toth model, the selectivity of CO_2/CH_4 and CO_2/N_2 was calculated to be 96 and 37, respectively. This effort will give rise to a new conception to tailor the charged MOF for high efficiency CO_2 adsorption and separation.

Introduction

The separation of carbon dioxide from gas mixtures containing methane is particularly important in both scientific research studies and industrial applications. Methane is the major component in many combustible gases, such as natural gas, biogas, coke oven gas, landfill gas, coal seam gas and straw syngas. Unfortunately, the coexistence of CO_2 in fuel gases will not only lower their calorific values but also cause pipeline and equipment corrosion.[1] As a greenhouse gas, release of CO_2 into the atmosphere should be avoided. Technologies including cryogenic distillation, membrane separation, chemical scrubbing, and physical adsorption have been attempted to separate CO_2 from CH_4.[2] Among these technologies, adsorption-based processes such as pressure-swing adsorption (PSA) and temperature-swing adsorption (TSA) are popular due to their low energy consumption and equipment cost.[3] Separation mechanisms of different systems can be divided into two types: equilibrium separation and kinetic separation. Equilibrium separation is based on the difference of maximum gas adsorption amounts in an equilibrium state. Kinetic separation is based on the special steric effect, such as concentrating O_2 from air on a carbon molecular sieve[4] or enrichment of CH_4 from coal-bed methane on Clinoptilolites[5] and zeolite ETS.[6] However, in these techniques, the widely used porous absorbents, such as zeolites and active carbons, meanwhile bear the drawbacks of either relatively low selectivity or small capacity of CO_2.[7]

Attractively, a new class of porous family, namely metal–organic frameworks (MOFs), has shined brilliantly on the aspect of CO_2 adsorption and separation in recent decades because of their structural diversities and numerous functionalities, such as the super-high surface area, tunable pore structures and functionalized pore walls and so on.[8] Since 2005, around 1400 papers relative to CO_2 adsorption and separation by MOFs have been published indexing from the ISI web of science, among which *ca.* 60% focus on CO_2 separation (Graph S1†). Generally, we can conceive six approaches to improve CO_2 separation as shown in Scheme 1, which may be suitable for other gas mixture separation techniques: (I) tuning of pore size contribution. Pore size contribution should be the most intuitive factor influencing the process of adsorptive separation. The predesigned pore sizes of MOFs can easily result in the controllable separation based on the difference of van der Waals diameters of the adsorbates. The separation mechanisms can be attributed to the molecular sieving effect, dynamic adsorption effect or

[a]College of Engineering, Peking University, Beijing 100871, China. E-mail: rzou@pku.edu.cn; Fax: +86-10-82529010; Tel: +86-10-82529045

[b]State Key Laboratory of Heavy Oil Processing, China University of Petroleum, Beijing, 102249, China

[c]College of Chemistry and Molecule Engineering, Zhengzhou University, Zhengzhou 450001, Henan, China

† Electronic supplementary information (ESI) available: ESI statistical result of CO_2 adsorption and separation (Graph S1), crystallographic data and structural refinement summary for compound **1** (Table S1), selected bond distances and angles for compound **1** (Table S2), crystal structure description (Fig. S1–S8), FTIR spectra (Fig. S9 and S10), TGA curves (Fig. S11), XRD data (Fig. S12), Langmuir fitting results for calculation of selectivity (Fig. S13–15), Toth fitting results for calculation of selectivity (Fig. S16–18), and calculation result of selectivity by the IAST method (Fig. S19). CCDC 967970 and 967971. For ESI and crystallographic data in CIF or other electronic format see DOI: 10.1039/c4ta01993h

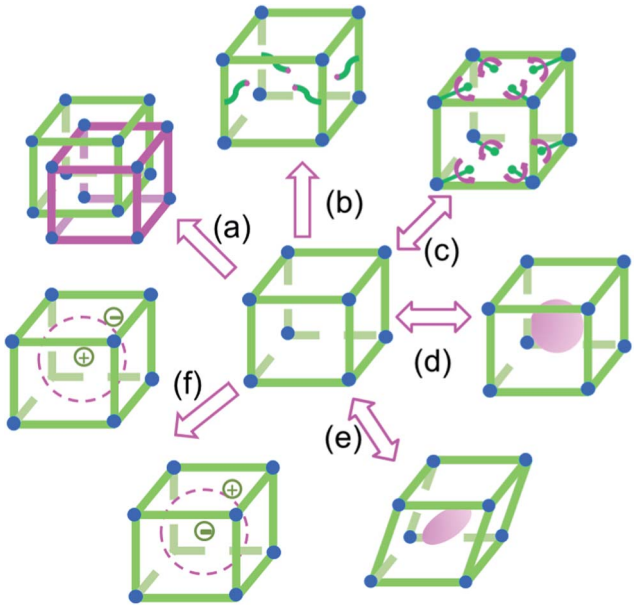

Scheme 1 Descriptions of the strategies to enhance CO_2/CH_4 selectivity. (a) Interpenetrating framework with ultramicropores; (b) functionalization of the pore environment; (c) utilization of open metal sites; (d) modification of large pores or channels; (e) breathing effect of the framework; (f) charged framework.

equilibrium adsorption effect. Recently, some new MOFs with ultramicroporous structures (<7 Å) showed promising properties for separating gases with similar molecular sizes,[9] in which interpenetration and catenation are frequently adopted to reduce the pore sizes of MOFs.[10] (II) Functionalization of pore walls. Modification of organic linkers on the pore walls is demonstrated to be another efficient method to enhance CO_2 uptakes and selectivity of the MOF materials, as well as reduction of pore sizes of MOF materials. The introduced functional groups and electron-rich atoms, including amidogens,[11] hydroxyl groups,[12] nitrogen atoms[13] and fluorine atoms,[14] exhibit remarkable intermolecular weak interaction with adsorbates by hydrogen bonding or electrostatic interactions. The functionalization can be easily realized through either directly self-assembly by using functional organic linkers or post-syntheses of MOF materials.[15] (III) Utilization of the vacancy of Lewis acid sites. The Lewis acid sites are the so-called unsaturatedly coordinated metal sites within MOFs. These open metal sites are often occupied by some small volatile molecules, such as water, methanol, *N*,*N*′-dimethylformamide (DMF), *etc.*, which can be easily removed or substituted without decomposition of the host frameworks of MOFs.[16,17] Recently, Long and his co-workers used ethanediamine to replace the bound DMF within Cu-BTTri for CO_2 adsorption. The result indicates that the ethanediamine modification can sharply enhance CO_2 uptakes of Cu-BTTri under low pressure.[18] (IV) Modification of the large pores or open channels. The large pores or channels of MOFs often lead to poor confinement with small gas molecules, as reflected by the low H_2 and CO_2 uptakes in MOF-177 compared with their analogies under low pressure.[19] However, modification of the large pores or channels by using functional small molecules, such as organic amine[20] and inorganic salts,[21] may be an efficient method to improve MOF performance. (V) Utilization of framework flexibility. It is worth noting that the framework flexibility of MOFs can also be employed for the selection adsorption of CO_2 for discovering the breathing effect of MIL-53 along with the change of pressure.[22] That is to say a contraction of the framework is induced by the strong interaction between polar functional groups and CO_2 molecules, and the pores reopen with the increase of pressure. (VI) Introduction of an electrostatic field. The design and synthesis of charged MOFs have received increasing attention.[23–26] The charged frameworks and counterion species may enhance the adsorbent–adsorbate interactions aroused by a strong electrostatic field in the cavity. Besides, the pore size and volume of the framework are adjustable by the post modification of cation exchange, leading to an ideal pore size for CO_2 condensation.[27–30] A molecular simulation result reported recently showed that the *rho* zeolite-like MOFs (*rho*-ZMOFs), a series of anionic frameworks, exhibit excellent selectivity of CO_2 from CH_4.[27]

It seems like that the strategy of the charged framework is similar to the well-known post-synthetic modification, both of which can enhance CO_2 capture by introducing extra zwitterions or functional groups into the framework. However, the post-synthetic work is not only tedious but also inefficient, for the small molecules which are expected to be incorporated into the inner part of the framework and are more likely to accumulate on the surface of the material. By contrast, the synthesis of the charged framework is much more convenient with the extra ions randomly and evenly distributed on the surface and the internal part of the framework. Herein, we report a novel ultramicroporous anionic MOF by the reaction of zinc acetate dihydrate and a new N-contained tricarboxylate ligand under solvothermal conditions, the formula of which was defined as $[Zn_3\mathbf{L}_2(HCOO)_{1.5}][(CH_3)_2NH_2]_{1.5}\cdot x$DMF, **1** ($H_3\mathbf{L}$ = 9-(4-carboxyphenyl)-9*H*-carbazole-3,6-dicarboxylic acid). The framework exhibits relatively high selectivity of CO_2 over CH_4 and N_2.

Experimental section

Synthesis

The solvents and reagents for synthesis were commercially available and used without further treatment. $H_3\mathbf{L}$ was synthesized by the classic Ullmann coupling procedure, followed by the F–C acylation reaction and the haloform reaction (Scheme 2).[31] In a typical preparation process of **1**, $Zn(CH_3COO)_2\cdot 2H_2O$ (0.1642 g, 0.75 mmol), $H_3\mathbf{L}$ (0.1891 g, 0.5 mmol), 80 mL DMF and 1 mL deionized water were placed in a 100 mL Teflon-lined steel autoclave. The autoclave was sealed, heated to 100 °C and kept at this temperature for two days, and then kept at 160 °C for another two days. After slowly cooling down to room temperature, pale yellow cubic crystals were obtained. The product was filtered out and washed with DMF.

Single-crystal X-ray crystallography

The crystal data were collected on a Bruker APEXII CCD Detector single-crystal X-ray diffractometer at room temperature with

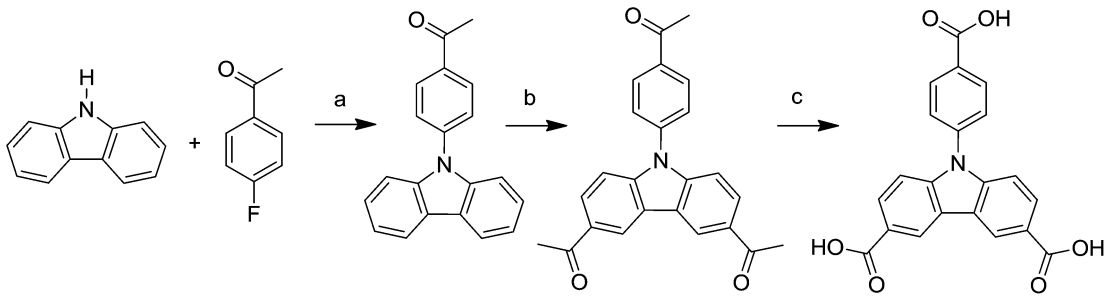

Scheme 2 Synthesis of H_3L. Reagents and conditions: (a) K_2CO_3, Cu, DMSO, 140 °C; (b) $AlCl_3$, acetyl chloride, CH_2Cl_2, RT; (c) liquid bromine, NaOH, *p*-dioxane–water, 60 °C.

Mo-Kα radiation ($\lambda = 0.71073$ Å).[32] The structures were solved by direct methods using the SHELXS program of the SHELXTL package and refined by full-matrix least-squares methods with SHELXL.[33] The Zn atom in **1** was located from the E-maps and other non-hydrogen atoms were located in successive difference Fourier syntheses, which were refined with anisotropic thermal parameters on F_2. The hydrogen atoms of the ligands were generated theoretically onto the specific atoms and refined isotropically with fixed thermal factors. Part solvent molecules in the structure were randomly dispersed, and thus their positions were impossible to refine using conventional discrete-atom models. To resolve these issues, the contribution of solvent electron density was removed by the SQUEEZE routine in PLATON.[34] Crystal data for **1**: monoclinic, space group *C*2/*c* with $a = 20.2644(6)$ Å, $b = 19.1216(7)$ Å, $c = 26.8248(9)$ Å, $\beta = 101.184(3)°$, $V = 10196.9(6)$ Å^3, $Z = 8$, $\rho_{calcd} = 1.435$ g cm^{-3}. Least-squares refinement based on 8998 reflections with $I > 2\sigma(I)$ and 611 parameters led to convergence, with a final $R_1 = 0.0786$, $R_{w2} = 0.2165$, and GOF = 1.021.†

Material characterization

Powder X-ray diffraction (PXRD) was performed on a Rigaku Dmax/2400 X-ray diffractometer operating at 40 kV and 100 mA, using Cu-Kα radiation ($\lambda = 1.5406$ Å). Thermogravimetric analysis (TGA) was carried out under a nitrogen atmosphere on a Q600 SDY TGA-DTA-DSC thermal analyzer from room temperature to 600 °C with a heating rate of 10 °C min^{-1}. Fourier Transform Infrared (FTIR) spectroscopy was carried out using an ECTOR22 Fourier transform infrared spectrometer between 400 and 4000 cm^{-1} in KBr pellets. Elemental analysis was performed on a Vario EL Elemental Analyzer. The cation exchange experiment was conducted by immersing **1a** in the saturated solution of $LiNO_3$ in fresh DMF, at room temperature. The sample was soaked for 24 h before decanting the metal nitrate solution. The obtained sample was rinsed and washed with DMF for three times to remove free $LiNO_3$.

Gas sorption measurements

Gas sorption data were collected by using a QUANTACHROME AUTOSORB-IQ gas adsorption analyzer. The temperature of the system was measured by using a high precision thermometer with an accuracy of 0.1 K and an error of 0.18%. The relative error of the system is 2.4%. The raw samples were activated under vacuum at 90 °C for 30 min and then at 150 °C for 300 min to obtain the solvent-free sample of **1a**. The N_2 sorption isomer was acquired in the pressure rage of P/P_0 from 0.01 to 0.99 at 77 K in a liquid nitrogen bath. The gas sorption experiments of CO_2 and CH_4 were conducted at 273 K in an ice-water bath.

Results and discussion

Synthesis

As is well-known, factors such as pH value, solvent, reaction time, temperature, templates and so on, all play very important roles in constructing MOFs materials during solvothermal reactions.[35] In this work, we discovered that the amount of water contained in the system is one of the vital factors that would influence the crystal growth of **1**. It should be noted that the high-temperature solvothermal reaction easily causes the hydrolysis of DMF,[36] and the hydrolyzates of formate and protonated dimethylamine (DMA^+) may participate in the construction of the MOF structure. Actually, quite a few charged MOFs, especially anionic ones, have *in situ* formed DMA^+ cations tapped in their pores or channels as counter-ions.[23,25,27,36–43] In this work, the existence of trace water can impact the hydrolysis of DMF and precipitation of **1**. Excess water may result in the formation of zinc formate byproducts.[36] Without water, only gel-like species was obtained at the bottom of the clarified liquid. On the other hand, temperature also plays an important role in obtaining a high purity product. Since the mixture of zinc acetate, H_3**L** and DMF turns out to be white slurry at room temperature, it was maintained at 100 °C for one day to become a clear solution, after which the temperature was increased to 160 °C for crystal growth. PXRD patterns of both the original and the solvent-free samples are consistent with the simulated one from the single crystal structure (Fig. S12†), indicating the high purity and the framework stability of **1**.

Crystal structure description

X-Ray crystallographic analysis indicates that **1** crystallizes in a monoclinic *C*2/*c* space group, consisting of an anionic $[Zn_6L_4(HCOO)_3]^{3-}$ framework and DMA^+ cations. The host framework is composed of three crystallographic independent Zn(II) coordinated to two **L** ligands and one and a half formate anions in

an asymmetric unit. Two symmetric Zn(1) ions are coupled to form a paddle-wheel building block by four carboxylate groups from four separate **L** ligands (Fig. 1a). Two terminal coordinate sites of the dinuclear cluster are occupied by two bridge formate anions. The Zn–Zn separation of 2.961(1) Å is a little longer than that of the reported Cu–Cu paddle wheel clusters.[44] Zn(2) adopts a slightly distorted octahedral coordination fashion with two *syn–syn* bridging formats and three carboxylate groups in *syn–syn* bridging and η-O, O′-μ-O, O modes, while Zn(3) has a five coordinate configuration with four carboxylate groups in *syn–syn* bridging, η_2, and η-O, O′-μ-O, O modes, respectively. The Zn(2) and Zn(3) are linked by three bridging carboxylate groups leading to dinuclear clusters with the closest separation of 3.244(1) Å (Fig. S1†). All Zn–O bond lengths fall into the normal range of 1.997–2.043 Å. Furthermore, the two types of dinuclear clusters are linked together by bridging formates in a 1 : 2 stoichiometric ratio.

The two crystallographic dependent L ligands coordinate five and six separate metal centers to lead a three-dimensional network with two types of molecular channels with dimensions of 4.0 × 4.8 and 4.2 × 8.0 $Å^2$, respectively. The corresponding protonated DMA^+ are trapped in the large channels (Fig. 1e). A detailed research of the location of DMA^+ demonstrates that the cations are connected to the host framework by hydrogen bonds (Fig. S2†), which further enhances the intrinsic stability of **1**. Notably, the centroid-to-centroid separations of the carbazole rings of two straggled L ligand pairs fall into the range of 3.243–3.573 Å (Fig. S3†), implying strong intermolecular π–π stacking interactions.[45]

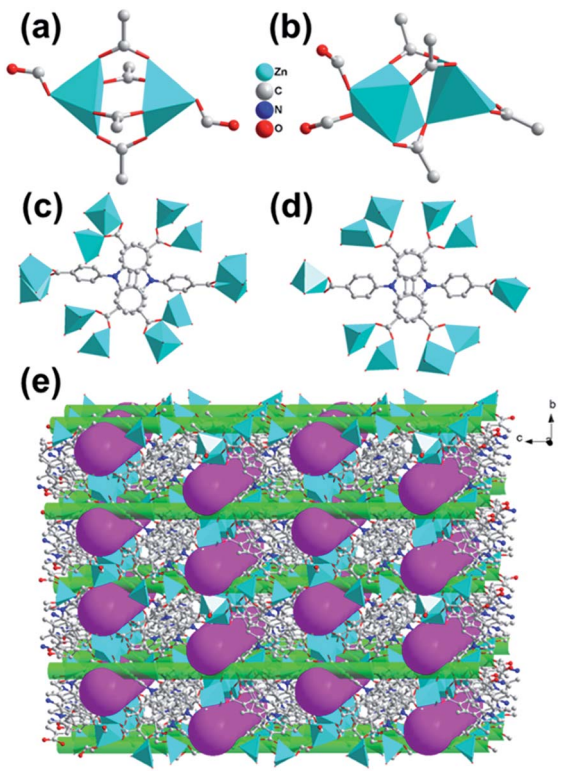

Fig. 1 View of (a) coordination environment of the symmetric paddle-wheel binuclear cluster; (b) asymmetric binuclear metal cluster; (c) ligand pair stacking by intermolecular π–π interaction as a 6-connected node with a torsional angle of 64.3(4); (d) ligand pair with a torsional angle of 54.6(4); (e) three-dimensional porous framework with two types of crossed channels. Pink: large channels blocked by DMA^+ along a direction and Green: small hollow channels along the *c* direction.

To better understand such a complicated structure, the topology of the anion framework of **1** was studied by using Topos 4.0 software.[46,47] The network topology is based on 3-connected (3-c) ligands and two types of 6-connected (6-c) metal clusters. The structure has a 3,6-connected (3,6-c) net with stoichiometry $(3\text{-c})_4(6\text{-c})_3$ (Fig. 2). Therefore, **1a** self-assembles into a new three-dimensional net with the point Schläfli symbol of $\{5;\ 6^2\}_2\{5^2;6\}_2\{5^3;6^4;7^6;8;9\}\{5^5;6^4;7^5;9\}_2$.

Property characterization

Thermogravimetric analysis of as synthesized **1** shows a significant decline before 200 °C, indicating the loss of solvents (Fig. S11†). The subsequent platform implies that **1** could keep stable below 400 °C, after which the framework collapsed according to the sharp decline of the curve. A detailed investigation of TGA curve of **1a** was then conducted. The slight decline before 250 °C is attributed to the loss of re-adsorbed water when exposed to an air atmosphere. The results are further confirmed by elemental analysis experiments, implying **1a** formulate as $[Zn_{3\mathbf{L}2}(HCOO)_{1.5}][(CH_3)_2NH_2]_{1.5}\cdot 3H_2O$ (observed (wt%): C 49.05, H 3.45, N 4.29; calculate (wt%): C 49.40, H 3.50, N 4.34). Theoretical weight loss for the coordinated water is 4.78%, which corresponds to the TGA result (4.11%). The subsequent weight loss of 7.01% from 250 to 400 °C is attributed to the decomposition of DMA^+ (theoretical weigh loss of 6.11%), which was reported to happen at around 300 °C.[38,48] It appears as a smooth slope rather than a step, which might result from the hydrogen bonds between DMA^+ and the framework.

Cation exchange experiment indicates that DMA^+ in the framework cannot be exchanged at room temperature, as proven by elemental analysis (Table S3†). We attributed this to the existence of hydrogen bonding interactions.

As seen in the PXRD pattern (Fig. S12†), the peak positions of **1a** are in good agreement with that of the simulated pattern, indicating that **1** retains its framework integrity after the removal of the guest molecule.

In the FTIR spectra of **1a** (Fig. S9 and S10†), the C–O vibration peak of carboxyl groups occurs at 1657 cm^{-1}, which is red-shifted compared with that of the free carboxyl groups of $H_3\mathbf{L}$. This shift was ascribed to the coordination of oxide atoms of carboxyl groups to metal ions. Another evidence of the formation of Zn–O coordination bonds is the sharply weakened peaks in the range of 3200–2500 cm^{-1}, which is corresponded to the binary associated hydroxyl. Specially, the peaks at 3430 and 1476 cm^{-1} correspond to the stretching vibration of N–H and C–N bonds in DMA^+, respectively, which further demonstrates its existence inside the framework.

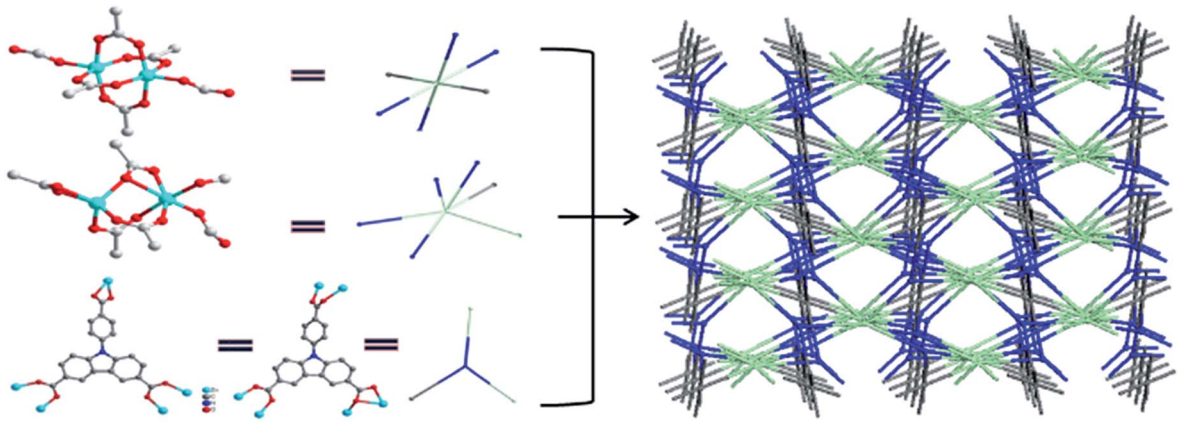

Fig. 2 Topological graph of the anion framework of **1**.

Gas sorption properties

The N_2 sorption isotherm of **1a** at 77 K exhibits a typical Type-I sorption behavior and reversible adsorption/desorption property with the largest uptake amount of 153.4 $cm^3\ g^{-1}$ (Fig. 2), demonstrating the permanent porosity of the framework. Dubinin–Radushkevich (DR) equation[49] gives the pore volume of 0.237 $cm^3\ g^{-1}$, which is comparable to the theoretical value of 0.241 $cm^3\ g^{-1}$ calculated by PLATON.[34] Moreover, the analysis of pore width distribution by the method of Horvath–Kawazoe (HK) shows that there are two types of ultramicropores with a dimension of 0.423 and 0.795 nm respectively, which is in good agreement with the crystal structure refinement result. The specific surface area is calculated to be 569.5 $m^2\ g^{-1}$ using the Brunauer–Emmett–Teller (BET) model, which is lower than that of other ultramicroporous frameworks with a similar pore size.[50] One possible reason is that DMA^+ cations blocked in the large channels prevent the entrance of N_2 molecules, leading to unavailability of the inner part of the channel. Moreover, this statement can also be used to illustrate the fact that the peak at 0.795 nm is much weaker than that at 0.423 nm in the figure of pore size distribution (Fig. 3).

Since the framework of **1a** has permanent porosity and the seemingly like pore controlled sorption property, its potential application on selective gas sorption can be expected. Here we studied the sorption behavior of CO_2, N_2 and CH_4 at 273 K (Fig. 4). The largest uptake amount of CO_2 is 57.5 $cm^3\ g^{-1}$ (2.57 $mmol g^{-1}$) at 1 atm, while that of N_2 (8.93 $cm^3\ g^{-1}$) and CH_4 (2.48 $cm^3\ g^{-1}$) is quite lower under the same conditions. Here, the adsorption amount of N_2 is abnormally higher than that of CH_4, which can be reasonably ascribed to the molecular sieve effect,[51] for the diameter of CH_4 (3.76 Å) molecular is a little larger than that of N_2 (3.646 Å).

The significant difference of uptake amounts makes **1a** great promise for the application of gas separation. Herein, we adopt four general methods: weight uptake ratio,[52] initial slope ratio,[53] dual-site Langmuir isotherm model and Toth model,[54] to calculate the selectivity (Table 1). Average selectivity of CO_2/CH_4 and CO_2/N_2 was calculated to be 77.2 and 22.2 respectively. To further explore the gas separation properties of **1a**, the Ideal Adsorbed Solution Theory (IAST) method was used to calculate the selectivities (see ESI†).[55,56] For an equimolar mixture of CO_2 and CH_4, the selectivity was calculated to be 87 at very low pressure (<0.1 mm Hg, Fig. S19†), which matches well with the

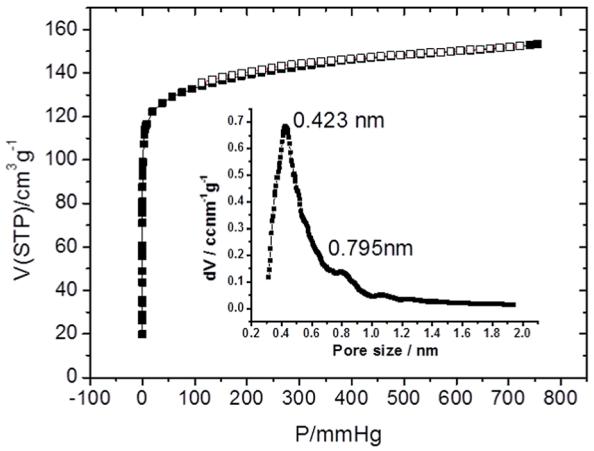

Fig. 3 N_2 sorption isotherms of **1a** at 77 K. Filled shapes: adsorption. Open shapes: desorption. Inset: pore size distribution calculated by the HK method.

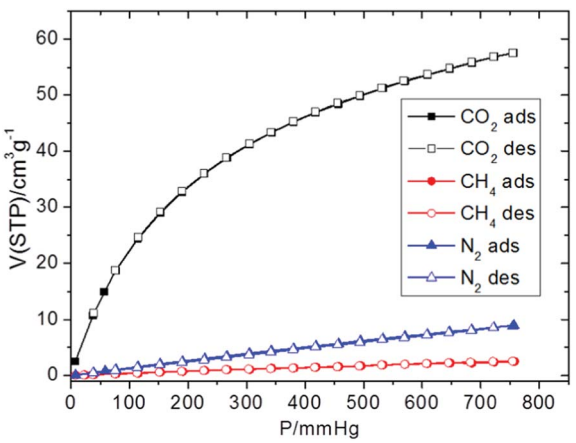

Fig. 4 CO_2, N_2 and CH_4 sorption isotherms of **1a** at 273 K. Filled shapes: adsorption. Open shapes: desorption.

Table 1 Selectivity of CO_2/CH_4 and CO_2/N_2 at 273 K

Calculation methods	CO_2/CH_4	CO_2/N_2
Langmuir model	85	25
Toth model	96	37
Initial slope ratio	64	17
Weight uptake ratio	64	10
Average	77.2	22.2
IAST	87[a], 1744[b]	24

[a] 2.6×10^{-5} bar, 50/50. [b] 1 bar, 50/50.

other calculation results. Interestingly, the selectivity increases sharply as the increase of pressure, which is quite different from other MOFs. The selectivity of CO_2/CH_4 reaches up to 1744 at atmosphere pressure, which is much higher than the ever reported charged and neutral MOFs listed in Table 2.[9,17,27–29,39,57–65] The satisfying high selectivity of CO_2 was attributed to the synergistic effect of pore size effect and the enhanced host–guest interaction caused by the immobile DMA^+. It is well-known that the kinetic diameter of CH_4 and N_2 is slightly larger than that of CO_2 (3.30 Å), and the similar size is one of the most important factor that hinders their separation. In the framework of **1a**, there are channels with different sizes: 0.423 and 0.795 nm. It is easy to understand that CH_4 and N_2 molecules are more difficult to pass through the small channels. Meanwhile, with DMA^+ inside, the remained pore space of large channels becomes too small to accommodate CH_4 and N_2 molecules. In addition, the existence of DMA^+ enhances the interaction between the host compound and CO_2 molecules. When flowing through small channels, CO_2 molecules interact strongly with DMA^+ ions blocking in the intercrossed large channels, thus the adsorption was enhanced. In contrast, the near-linear adsorption isotherms of CH_4 and N_2 are indicative of their low affinity to the charged framework, which can be expected from its relatively low polarizability.

In the three gas sorption isotherms of N_2, CO_2, CH_4, desorption curves almost completely coincide with corresponding adsorption curves. Without hysteretic desorption behaviour, the framework is bound to be unreformed and the pore structure should be maintained during the sorption test, which further confirms the rigidity of **1**. Therefore, its application in gas storage and separation, especially CO_2/CH_4 separation for natural gas purification, can be energetically expected.

Conclusions

In conclusion, a novel charged MOF was prepared and exhibited relatively potential high selectivity of CO_2 over CH_4 and N_2. In addition to the pore size effect, extra framework DMA^+ may largely enhance the host–guest interaction during the adsorption of CO_2. The results reveal that anionic frameworks with an appropriate pore size are excellent candidates for gas

Table 2 CO_2 separation properties of some MOFs[a]

	Selectivity						
MOFs	CO_2/CH_4	CO_2/N_2	C_{CO_2}/%	E/S	T/K	P/bar	Ref.
Mg(dobdc)$_2$/Mg-MOF-74	283	_	_	E	298	1	17
	_	800	_	_	313	1	58
rho-ZMOF	80	_	50	S	298	1	27
	_	500	15	S	298	1	27
rho-ZMOF	_	22.6	_	E	298	1	29
sod-ZMOF	_	20.4	_	E	298	1	29
ZIF-78	10.6	50.1	50	E	298	1	57
$Zn_2(bpdc)_2(bpee)(DMF)_2$	257	_	_	E	298	0.16	59
	_	116	_	E	298	1	59
SNU-151/$[Zn_5(NTN)_4(DEF)_2][NH_2(C_2H_5)_2]_2$	7.2	_	50	E	298	1	39
	_	30	15	E	298	1	39
SIFSIX-2-Cu-i	33/51	_	50	E	298	1	9
	_	140/72	10	E	298	1	9
SIFXIX-3-Zn	231/305	_	50	E	298	1	9
	_	1818/1700	10	E	298	1	9
100Ksod-ZMOF	_	172.74	_	S	308	10	28
UTSA-16/$[K(H_2O)_2Co_3(cit)(Hcit)]$	29.8		50	E	296	2	60
	_	314.7	15	E	296	2	60
mmenCuBTTri	_	329.0	15	E	296	2	60
Compound **1**	1744	_	50	S	273	1	This work
	_	25	15	S	273	1	This work
azo-COP-3	_	288.1	15	S	323	1	61
Polyamine-tethered PPNs	_	442	15	S	295	1	62
POP(2)	_	155	10	S	298	1	63
FCTF-1-600	_	19/152	10	S/E	298	1	64

[a] C_{CO_2}/%: concentration of CO_2; E/S: experiment/simulation.

separation. Further study is expected to design and synthesize new types of charged frameworks with *in situ* formed counter ions. With one kind of species randomly distributed into another, the charged MOF can be considered as "composite material", and its "one-pot" method is inspirational to the synthesis methodology.

Acknowledgements

This work was supported by the National Natural Science Foundation of China (11175006, 51322205 and 21371014), the Ministry of Education program for New Century Excellent Talents of China (NCET-11-0027), and the Singapore-Peking University SPURc program.

Notes and references

1 R. W. Baker, *Ind. Eng. Chem. Res.*, 2002, **41**, 1393–1411.
2 D. M. D'Alessandro, B. Smit and J. R. Long, *Angew. Chem., Int. Ed.*, 2010, **49**, 6058–6082.
3 G. D. Pirngruber, L. Hamon, S. Bourrelly, P. L. Llewellyn, E. Lenoir, V. Guillerm, C. Serre and T. Devic, *ChemSusChem*, 2012, **5**, 762–776.
4 T. R. Gaffney, *Curr. Opin. Solid State Mater. Sci.*, 1996, **1**, 69–75.
5 A. Jayaraman, A. J. Hernandez-Maldonado, R. T. Yang, D. Chinn, C. L. Munson and D. H. Mohr, *Chem. Eng. Sci.*, 2004, **59**, 2407–2417.
6 A. Ansón, S. M. Kuznicki, T. Kuznicki, T. Haastrup, Y. Wang, C. C. H. Lin, J. A. Sawada, E. M. Eyring and D. Hunter, *Microporous Mesoporous Mater.*, 2008, **109**, 577–580.
7 J. McEwen, J. D. Hayman and A. O. Yazaydin, *Chem. Phys.*, 2013, **412**, 72–76.
8 K. Sumida, D. L. Rogow, J. A. Mason, T. M. McDonald, E. D. Bloch, Z. R. Herm, T.-H. Bae and J. R. Long, *Chem. Rev.*, 2012, **112**, 724–781.
9 P. Nugent, Y. Belmabkhout, S. D. Burd, A. J. Cairns, R. Luebke, K. Forrest, T. Pham, S. Ma, B. Space, L. Wojtas, M. Eddaoudi and M. J. Zaworotko, *Nature*, 2013, **495**, 80–84.
10 B. Liu, L. X. Tang, Y. H. Lian, Z. Li, C. Y. Sun and G. J. Chen, *Acta Chim. Sin.*, 2013, **71**, 920–928.
11 S. Vaesen, V. Guillerm, Q. Y. Yang, A. D. Wiersum, B. Marszalek, B. Gil, A. Vimont, M. Daturi, T. Devic, P. L. Llewellyn, C. Serre, G. Maurin and G. De Weireld, *Chem. Commun.*, 2013, **49**, 10082–10084.
12 I. Spanopoulos, P. Xydias, C. D. Malliakas and P. N. Trikalitis, *Inorg. Chem.*, 2013, **52**, 855–862.
13 P. Z. Li and Y. L. Zhao, *Chem.–Asian J.*, 2013, **8**, 1680–1691.
14 D.-X. Xue, A. J. Cairns, Y. Belmabkhout, L. Wojtas, Y. Liu, M. H. Alkordi and M. Eddaoudi, *J. Am. Chem. Soc.*, 2013, **135**, 7660–7667.
15 Q. J. Yan, Y. C. Lin, P. Y. Wu, L. Zhao, L. J. Cao, L. M. Peng, C. L. Kong and L. Chen, *ChemPlusChem*, 2013, **78**, 86–91.
16 H. Xu, Y. B. He, Z. J. Zhang, S. C. Xiang, J. F. Cai, Y. J. Cui, Y. Yang, G. D. Qian and B. L. Chen, *J. Mater. Chem. A*, 2013, **1**, 77–81.
17 Z. Bao, L. Yu, Q. Ren, X. Lu and S. Deng, *J. Colloid Interface Sci.*, 2011, **353**, 549–556.
18 A. Demessence, D. M. D'Alessandro, M. L. Foo and J. R. Long, *J. Am. Chem. Soc.*, 2009, **131**, 8784–8786.
19 J. L. C. Rowsell, A. R. Millward, K. S. Park and O. M. Yaghi, *J. Am. Chem. Soc.*, 2004, **126**, 5666–5667.
20 T. M. McDonald, W. R. Lee, J. A. Mason, B. M. Wiers, C. S. Hong and J. R. Long, *J. Am. Chem. Soc.*, 2012, **134**, 7056–7065.
21 Z. J. Zhang, W. Y. Gao, L. Wojtas, S. Q. Ma, M. Eddaoudi and M. J. Zaworotko, *Angew. Chem., Int. Ed.*, 2012, **51**, 9330–9334.
22 B. Zornoza, A. Martinez-Joaristi, P. Serra-Crespo, C. Tellez, J. Coronas, J. Gascon and F. Kapteijn, *Chem. Commun.*, 2011, **47**, 9522–9524.
23 A. K. Chaudhari, S. Mukherjee, S. S. Nagarkar, B. Joarder and S. K. Ghosh, *CrystEngComm*, 2013, **15**, 9465–9471.
24 P. He, H. Liu, Y. F. Li, Z. G. Lei, S. P. Huang, P. Wang and H. P. Tian, *Mol. Simul.*, 2012, **38**, 72–83.
25 T. Li and N. L. Rosi, *Chem. Commun.*, 2013, **49**, 11385–11387.
26 R. Babarao, M. Eddaoudi and J. W. Jiang, *Langmuir*, 2010, **26**, 11196–11203.
27 R. Babarao and J. W. Jiang, *J. Am. Chem. Soc.*, 2009, **131**, 11417–11425.
28 B. Demir and M. G. Ahunbay, *J. Phys. Chem. C*, 2013, **117**, 15647–15658.
29 C. Chen, J. Kim, D. A. Yang and W. S. Ahn, *Chem. Eng. J.*, 2011, **168**, 1134–1139.
30 Y. F. Chen, A. Nalaparaju, M. Eddaoudi and J. W. Jiang, *Langmuir*, 2012, **28**, 3903–3910.
31 S. B. Choi, M. J. Seo, M. Cho, Y. Kim, M. K. Jin, D.-Y. Jung, J.-S. Choi, W.-S. Ahn, J. L. C. Rowsell and J. Kim, *Cryst. Growth Des.*, 2007, **7**, 2290–2293.
32 T. Higashi, *Program for Absorption Correction*, Rigaku Corporation, Tokyo, Japan, 1995.
33 G. M. Sheldrick, *SHELXTL NT, Program for Solution and Refinement of Crystal Structures, Version 5.1*, University of Göttingen, Göttingen, Germany, 1997.
34 A. L. Spek, *PLATON, A Multipurpose Crystallographic Tool*, Utrecht University, Utrecht, The Netherlands, 2001.
35 N. Stock and S. Biswas, *Chem. Rev.*, 2012, **112**, 933–969.
36 A. D. Burrows, K. Cassar, R. M. W. Friend, M. F. Mahon, S. P. Rigby and J. E. Warren, *CrystEngComm*, 2005, **7**, 548–550.
37 E. Q. Procopio, F. Linares, C. Montoro, V. Colombo, A. Maspero, E. Barea and J. A. R. Navarro, *Angew. Chem., Int. Ed.*, 2010, **49**, 7308–7311.
38 Y.-X. Tan, Y.-P. He and J. Zhang, *Chem. Commun.*, 2011, **47**, 10647.
39 M.-H. Choi, H. J. Park, D. H. Hong and M. P. Suh, *Chem.–Eur. J.*, 2013, **19**, 17432–17438.
40 Q.-G. Zhai, Q. Lin, T. Wu, L. Wang, S.-T. Zheng, X. Bu and P. Feng, *Chem. Mater.*, 2012, **24**, 2624–2626.
41 S. M. Chen, J. Zhang, T. Wu, P. Y. Feng and X. H. Bu, *J. Am. Chem. Soc.*, 2009, **131**, 16027–16029.
42 D. Peralta, G. Chaplais, A. Simon-Masseron, K. Barthelet, C. Chizallet, A. A. Quoineaud and G. D. Pirngruber, *J. Am. Chem. Soc.*, 2012, **134**, 8115–8126.

43 Y. Liu, V. C. Kravtsov, R. Larsen and M. Eddaoudi, *Chem. Commun.*, 2006, 1488–1490.
44 R.-Q. Zou, H. Sakurai, S. Han, R.-Q. Zhong and Q. Xu, *J. Am. Chem. Soc.*, 2007, **129**, 8402–8403.
45 R. Zou, A. I. Abdel-Fattah, H. Xu, A. K. Burrell, T. E. Larson, T. M. McCleskey, Q. Wei, M. T. Janicke, D. D. Hickmott, T. V. Timofeeva and Y. Zhao, *Cryst. Growth Des.*, 2010, **10**, 1301–1306.
46 M. O'Keeffe, M. A. Peskov, S. J. Ramsden and O. M. Yaghi, *Acc. Chem. Res.*, 2008, **41**, 1782–1789.
47 S. R. Batten, N. R. Champness, X.-M. Chen, J. Garcia-Martinez, S. Kitagawa, L. Öhrström, M. O'Keeffe, M. Paik Suh and J. Reedijk, *Pure Appl. Chem.*, 2013, **85**, 1715–1724.
48 M. E. Medina, Y. Dumont, J.-M. Grenèche and F. Millange, *Chem. Commun.*, 2010, **46**, 7987–7989.
49 A. Gil and P. Grange, *Colloids Surf., A*, 1996, **113**, 39–50.
50 Z. Lin, R. Zou, J. Liang, W. Xia, D. Xia, Y. Wang, J. Lin, T. Hu, Q. Chen, X. Wang, Y. Zhao and A. K. Burrell, *J. Mater. Chem.*, 2012, **22**, 7813–7818.
51 S. Cavenati, C. A. Grande and A. E. Rodrigues, *J. Chem. Eng. Data*, 2004, **49**, 1095–1101.
52 T. K. Kim and M. P. Suh, *Chem. Commun.*, 2011, **47**, 4258–4260.
53 R. Banerjee, H. Furukawa, D. Britt, C. Knobler, M. O'Keeffe and O. M. Yaghi, *J. Am. Chem. Soc.*, 2009, **131**, 3875–3877.
54 Z. X. Chen, S. C. Xiang, H. D. Arman, J. U. Monda, P. Li, D. Y. Zhao and B. L. Chen, *Inorg. Chem.*, 2011, **50**, 3442–3446.
55 A. L. Myers and J. M. Prausnitz, *AIChE J.*, 1965, **11**, 121–127.
56 B. P. Bering and V. V. Serpenskii, *Zh. Fiz. Khim.*, 1952, **26**, 253–269.
57 A. Phan, C. J. Doonan, F. J. Uribe-Romo, C. B. Knobler, M. O'Keeffe and O. M. Yaghi, *Acc. Chem. Res.*, 2009, **43**, 58–67.
58 Z. R. Herm, J. A. Swisher, B. Smit, R. Krishna and J. R. Long, *J. Am. Chem. Soc.*, 2011, **133**, 5664–5667.
59 H. Wu, R. S. Reali, D. A. Smith, M. C. Trachtenberg and J. Li, *Chem.–Eur. J.*, 2010, **16**, 13951–13954.
60 S. Xiang, Y. He, Z. Zhang, H. Wu, W. Zhou, R. Krishna and B. Chen, *Nat. Commun.*, 2012, **3**, 954–963.
61 H. A. Patel, S. H. Je, J. Park, D. P. Chen, Y. Jung, C. T. Yavuz and A. Coskun, *Nat. Commun.*, 2013, **4**, 1357.
62 W. Lu, J. P. Sculley, D. Yuan, R. Krishna, Z. Wei and H. C. Zhou, *Angew. Chem., Int. Ed.*, 2012, **51**, 7480–7484.
63 V. Guillerm, L. J. Weselinski, M. Alkordi, M. I. Mohideen, Y. Belmabkhout, A. J. Cairns and M. Eddaoudi, *Chem. Commun.*, 2014, **50**, 1937–1940.
64 Y. Zhao, K. X. Yao, B. Teng, T. Zhang and Y. Han, *Energy Environ. Sci.*, 2013, **6**, 3684–3692.
65 J. Liu, P. K. Thallapally, B. P. McGrail, D. R. Brown and J. Liu, *Chem. Soc. Rev.*, 2012, **41**, 2308–2322.